STEM CELLS®

EMBRYONIC STEM CELLS/INDUCED PLURIPOTENT STEM CELLS

PRMT1 and PRMT8 Regulate Retinoic Acid-Dependent Neuronal Differentiation with Implications to Neuropathology

ZOLTAN SIMANDI,[a] ERIK CZIPA,[a] ATTILA HORVATH,[a] ARON KOSZEGHY,[b] CSILLA BORDAS,[b] SZILARD PÓLISKA,[a] ISTVAN JUHASZ,[c,d] LASZLÓ IMRE,[e] GABOR SZABÓ,[e] BALAZS DEZSO,[f] ENDRE BARTA,[a] SASCHA SAUER,[g] KATALIN KAROLYI,[h] ILONA KOVACS,[h] GABOR HUTÓCZKI,[i] LASZLÓ BOGNAR,[i] ALMOS KLEKNER,[i] PETER SZUCS,[b,j] BALINT L. BALINT,[a] LASZLO NAGY[a,k,l]

Key Words. PRMT1 • PRMT8 • Retinoid signaling • Neural differentiation • Glioblastoma

[a]Department of Biochemistry and Molecular Biology, [b]Department of Physiology, [c]Department of Dermatology, [d]Department of Surgery and Operative Techniques, Faculty of Dentistry, [e]Department of Biophysics and Cell biology, [f]Department of Pathology, [i]Department of Neurosurgery, [j]MTA-DE-NAP B-Pain Control Group, and [k]MTA-DE "Lendulet" Immunogenomics Research Group, University of Debrecen, Debrecen, Hungary; [g]Otto Warburg Laboratory, Max Planck Institute for Molecular Genetics, Berlin, Germany; [h]Department of Pathology, Kenézy Hospital and Outpatient Clinic, Debrecen, Hungary; [l]Sanford-Burnham Medical Research Institute at Lake Nona, Orlando, Florida, USA

Correspondence: Laszlo Nagy, MD, PhD, 6400 Sanger Road, Orlando, Florida 32827, USA. Telephone: +1-407-745-2150; Fax: +1-407-745-2013; e-mail: lnagy@sanfordburnham.org

Received June 25, 2014; accepted for publication October 22, 2014; first published online in STEM CELLS *EXPRESS* November 11, 2014.

1066-5099/2014/$30.00/0

http://dx.doi.org/10.1002/stem.1894

ABSTRACT

Retinoids are morphogens and have been implicated in cell fate commitment of embryonic stem cells (ESCs) to neurons. Their effects are mediated by RAR and RXR nuclear receptors. However, transcriptional cofactors required for cell and gene-specific retinoid signaling are not known. Here we show that protein arginine methyl transferase (PRMT) 1 and 8 have key roles in determining retinoid regulated gene expression and cellular specification in a multistage neuronal differentiation model of murine ESCs. PRMT1 acts as a selective modulator, providing the cells with a mechanism to reduce the potency of retinoid signals on regulatory "hotspots." PRMT8 is a retinoid receptor target gene itself and acts as a cell type specific transcriptional coactivator of retinoid signaling at later stages of differentiation. Lack of either of them leads to reduced nuclear arginine methylation, dysregulated neuronal gene expression, and altered neuronal activity. Importantly, depletion of PRMT8 results in altered expression of a distinct set of genes, including markers of gliomagenesis. PRMT8 is almost entirely absent in human glioblastoma tissues. We propose that PRMT1 and PRMT8 serve as a rheostat of retinoid signaling to determine neuronal cell specification in a context-dependent manner and might also be relevant in the development of human brain malignancy. STEM CELLS *2015;33:726–741*

INTRODUCTION

Animal cells in developing embryos receive positional signals from diffusible molecules, called morphogens. Retinoic acid (RA), a natural metabolite of vitamin A, has been proposed to be a vertebrate morphogen [1, 2]. Molecularly, RA acts via the activation of Retinoic Acid Receptor : Retinoid X Receptor (RAR:RXR) heterodimers. RARs and RXRs are two subfamilies of nuclear receptors (NRs) that bind to DNA motifs called RA-response elements (RAREs), typically arranged as direct repeats (DR) and regulate transcription [3]. Unliganded RAR:RXR heterodimers bind to corepressor complexes and are thought to maintain target genes in a repressed state [4]. Ligand binding stimulates a cascade of events resulting in the release of the corepressor complexes, recruitment of transcriptional coactivators, and thus initiation of transcription [5, 6]. However, the composition of coactivator and corepressor complexes is cell-type and context dependent and contributes to cell specification and potentially gene-specific transcription [7].

Members of the protein arginine methyl transferase (PRMT) family have been shown to act as nuclear receptor coactivators [8–11]. Based on their enzyme activity PRMTs are grouped into three groups. Type I enzymes (PRMT1, 2, 3, 4, 6, and 8) catalyze the formation of asymmetric dimethylarginine (aDMA) residues while the type II (PRMT5) enzyme catalyze the formation of symmetric dimethylarginine (sDMA) residues. Both type I and II enzymes generate monomethylarginine (MMA) intermediates. The type III enzyme (PRMT7) only generates a MMA mark [12].

Importantly, asymmetric arginine methylation is associated with cellular differentiation [13, 14]. Early studies revealed high level of aDMA in the nervous system [15], however expression profile of type I PRMTs and their functional contribution to neurogenesis remained largely uncharacterized [16–19].

PRMT1 is a major type of protein arginine methyltransferase and the most studied one [20]. Importantly, PRMT1 null mice die at an early stage, indicating its essential role in embryonic development [17]. PRMT1-dependent

methylation of Arg3 on H4 tail peptides facilitates P300-mediated histone H4 acetylation in vitro [21–23]. These studies collectively suggest that PRMT1 is likely to collaborate with P300 to regulate transcription.

Mechanistically, PRMT1 dimerization/oligomerization or heterodimerization may be required for PRMT1 to achieve its coactivator function [24]. A comparison of mammalian PRMTs revealed that PRMT8 is PRMT1's closest paralog within this enzyme family, with an identical exon structure and a brain specific expression pattern and can form a heterodimer with PRMT1 [25].

In this work, we explored the mechanistic and functional role of PRMT1 and PRMT8 using a multistage differentiation model of mouse embryonic stem cells (ESCs) to neurons. Our findings implicate asymmetric arginine methylation as a novel way to regulate the potency of retinoic acid regulated transcriptional response. We show that PRMT1 and PRMT8 are linked and act as part of a rheostat to integrate retinoid signaling into neuronal specific gene expression governed by retinoids with implications to neurological disorders.

Materials and Methods

Additional details about all of the mehods listed below, information about the antibodies used and related citations can be found in the Supporting Information/Extended Experimental Procedures.

Mouse ESC Culture and Neural Differentiation

Wild type and genetically modified (see in the text) mouse ESCs (mESCs) (kind gift of Tomo Saric and Istvan Szatmari) were cultured on 0.1% gelatin-coated plates in feeder-free condition in 5% CO_2 at 37°C. Cells were differentiated through embryoid body (EB) formation [26].

Ligands and Treatment

Cells were treated with vehicle (dimethylsulfoxide) or with the following ligands: LG268 (a gift from R. Heyman; Ligand Pharmaceuticals, San Diego, CA), RA (Sigma-Aldrich, St. Louis, MO), or AM580 [27].

Gene Silencing Assays

Small hairpin RNA (shRNA) lentiviral plasmids (MISSION shRNA, TRCN0000018490-493 and TRCN0000097479-482) were purchased from Sigma (Sigma-Aldrich, St. Louis, MO) for targeting the mouse PRMT1 and PRMT8, respectively.

Chromosome Counting

Cells were treated with colcemid (Sigma-Aldrich, St. Louis, MO) for mitotic arrest and harvested by standard hypotonic treatment and methanol: acetic acid (3:1) fixation. Slides were prepared by standard air-drying method. Twenty DAPI (4′, 6 -Diamidino-2-phenylindole) stained chromosomal spreads were counted in each case.

Teratoma Assay

mESCs were trypsinized and resuspended in 0.9% normal saline at a concentration of 5×10^6 cells per ml. Severe combined immunodeficiency (SCID) mice were anesthetized, and 100 μl of the cell suspension was injected into the lower leg. After 4–6 weeks, the teratomas were surgically dissected, fixed, embedded in paraffin, and sectioned. The sections were then hematoxylin and eosin stained.

Real-Time Quantitative Reverse Transcriptase Polymerase Chain Reaction

Total RNA was isolated with TRIZOL reagent (Invitrogen, Carlsbad, CA, http://www.invitrogen.com). cDNA synthesis was performed with High Capacity cDNA Reverse Trancription kit (Applied Biosystems, Foster City, CA, http://www.appliedbiosystems.com) according to the manufacturer's recommendation. Quantitative polymerase chain reaction (PCR) was performed using real-time PCR (ABI PRISM 7900, Applied Biosystems). Gene expression was quantified by the comparative C_T method and normalized to Gapdh. Values are expressed as mean $\pm$ SD of the mean. GraphPad Prism version 5.02 was used for data interpretation. The sequences of the primers and probes are available upon request.

Calcium Imaging, Loose-Patch and Whole-Cell Patch-Clamp Recording

ESCs were differentiated to neurons for 16 days. Whole cell patch clamp and calcium imaging experiments were conducted on these cells to investigate their functional properties. For the measurement of intracellular calcium concentration changes, cells were and loaded with the calcium indicator dye Oregon Green 488 BAPTA-1, AM. Calcium imaging measurements were carried out as described by Koszeghy et al. [28] with minor modifications. Patch clamp experiments were conducted similarly as in Koszeghy et al. [28] with some alterations.

RNA-seq and Analysis

RNA-Seq library was prepared from two biological replicates by using TruSeq RNA Sample Preparation Kit (Illumina) according to manufacturer's protocol. Illumina RNA-sequencing was performed using standard procedures at the Centre National de Genotypage (CNG) Paris, France.

The TopHat-Cufflinks-CummeRbund toolkit trio was used for mapping spliced reads, making transcript assemblies, and getting, sorting, and visualizing gene expression data. Series accession number: SRP042072 / PRJNA248061.

Microarray Analysis

Data have been analyzed using GeneSpring v12.6. All microarray data from this study have been submitted to the Gene Expression Omnibus (Series accession number: GSE37060 and GSE37060). Gene lists were imported into IPA (Ingenuity Systems, www.ingenuity.com) to carry out pathway analysis.

Enrichment of Histone Modification

Cells were washed and labeled with rabbit anti-H4R3me2a primary antibody diluted ×800 in 1% Bovine Serum Albumin/1×Phosphate Buffer Saline/5 mM EDTA at 4°C overnight using a total volume of 150 μl labeling solution on each slides. Data evaluation and hardware control were performed by the iCys 3.4 software for Windows XP.

Chromatin Immunoprecipitation and Sequencing

Chromatin immunoprecipitation (ChIP)-qPCR and ChIP-seq experiments were carried out as previously described [29], with minor modifications. Primary analysis of the ChIP-seq raw reads has been carried out using the ChIP-seq analyze

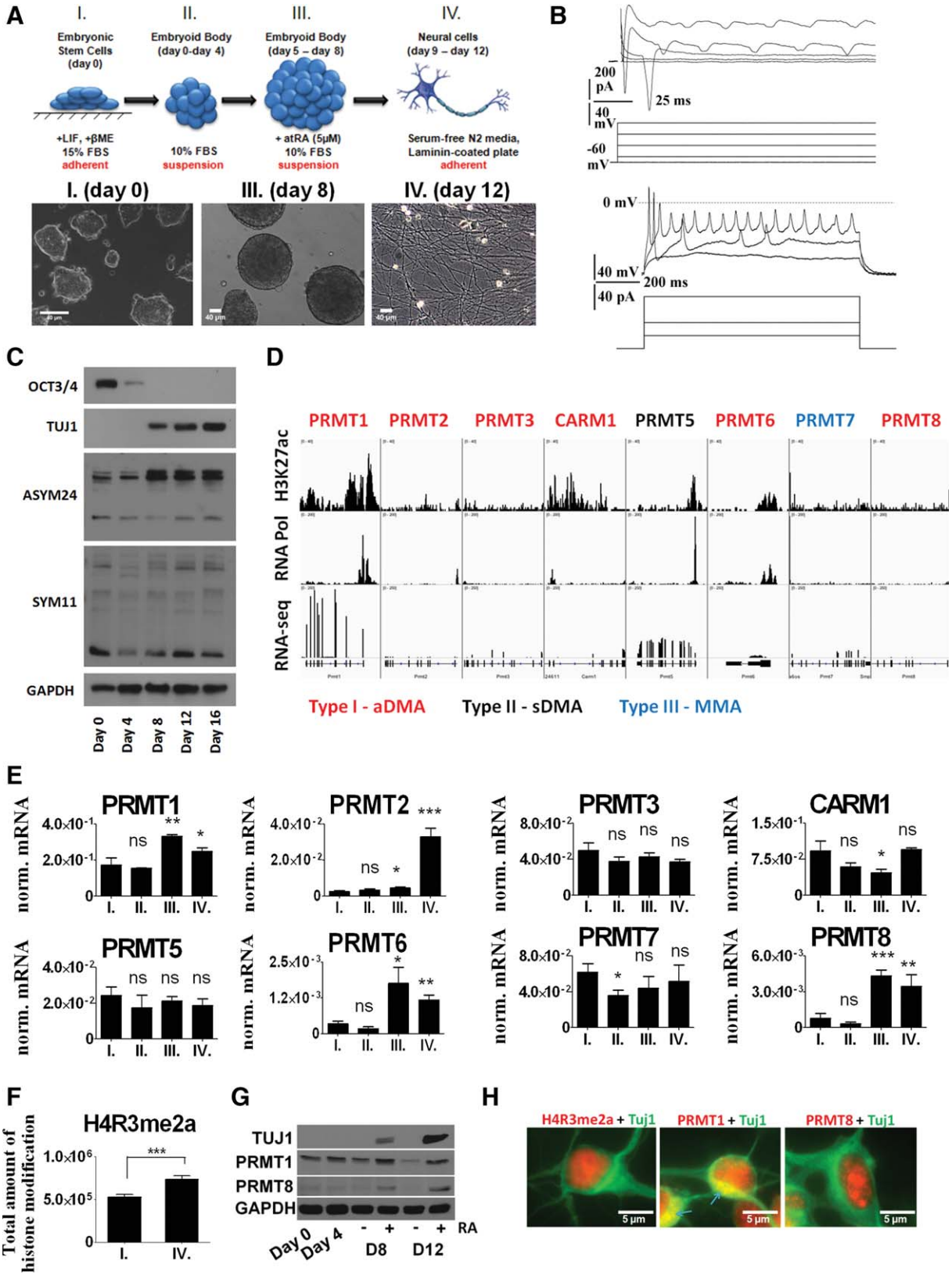
A
I.
Embryonic Stem Cells (day 0)
II.
Embryoid Body (day 0-day 4)
III.
Embryoid Body (day 5 – day 8)
IV.
Neural cells (day 9 – day 12)
+LIF, +βME 15% FBS adherent
10% FBS suspension
+ atRA (5μM) 10% FBS suspension
Serum-free N2 media, Laminin-coated plate adherent
I. (day 0)
III. (day 8)
IV. (day 12)
B
200 pA
25 ms
40 mV
-60 mV
0 mV
40 mV
200 ms
40 pA
C
OCT3/4
TUJ1
ASYM24
SYM11
GAPDH
Day 0
Day 4
Day 8
Day 12
Day 16
D
PRMT1 PRMT2 PRMT3 CARM1 PRMT5 PRMT6 PRMT7 PRMT8
H3K27ac
RNA Pol
RNA-seq
Type I - aDMA
Type II - sDMA
Type III - MMA
E
PRMT1
PRMT2
PRMT3
CARM1
PRMT5
PRMT6
PRMT7
PRMT8
norm. mRNA
I. II. III. IV.
F
H4R3me2a
Total amount of histone modification
I. IV.
G
TUJ1
PRMT1
PRMT8
GAPDH
Day 0 Day 4 D8 D12
RA
H
H4R3me2a + Tuj1
PRMT1 + Tuj1
PRMT8 + Tuj1
5 μm

Figure 1.

command line pipeline. IGV (Integrative Genomics Viewer) was used for data visualization. All ChIP-seq data from this study have been submitted to the Sequence Read Archive, NCBI (Series accession number: SRP042072/PRJNA248061).

Tissue Samples

Glioblastoma and normal brain tissues were collected during neurosurgical operations in the Department of Neurosurgery, University of Debrecen. Normal samples were collected either during functional neurosurgery for epilepsy or nontumor herniated brain tissue during tumor surgery. Sections for histological analysis were cut from the same samples used for mRNA analysis. All procedures were approved by the National Ethical Committee, and every patient signed an informed consent form.

Results

Asymmetric Arginine Methylation Is Present in Distinct Stages of RA-Induced Neural Differentiation

To explore the involvment of arginine methylation in neuronal development, we set up an ESC-based model system (Fig. 1A). The four stages are: (I) undifferentiated ESCs, (II) aggregates of spontaneously differentiating cells (termed EBs), (III) cells commited to neuroectoderm as a result of all-trans RA treatment, and (IV) the fully differentiated neuronal cells [26]. Importantly, these terminally differentiated neurons have electrophysiological properties similar to those brain-derived neurons and show positive staining for synapsin (Fig. 1B; Supporting Information Fig. S1A), this is in line with the findings of others on ESC derived neurons differentiated using the same method [30].

This model system allows a systematic step-by-step analysis of early cell fate commitment as well as late neural cell type specification. As Supporting Information Figure S1B shows, these stages can be characterized by distinct gene expression signatures. Undifferentiated ESCs express high level of stem cell specific Oct3/4 [31], while upon induction of spontaneous differentiation the level of Oct3/4 is declining. Treatment with RA causes the activation of RA signaling as it is reflected by the increased Rarβ expression. At this stage, cells become Pax6-positive neural progenitor cells with the characteristics of radial glial cells [26]. Members of the Hox-family, such as Hoxb1, are also induced. In the last stage, high expression of Tuj1 and Dcx, two well-established markers of neurogenesis can be detected [32].

Using this multistage differentiation system, we have found that proteins with sDMA and aDMA residues are present in ESCs (Fig. 1C; Supporting Information Fig. S1C). Asymmetric arginine methylation level of these proteins was changing dynamically during RA-induced neural differentiation, suggesting either an increased level of target proteins or overall type I enzyme activity. A 68-kDa protein (likely Sam68, a previously identified arginine methyltransferase target) [33] showed dramatically increased Asym24 level. Increased expression of Sam68 during neural differentiation could be also detected (Supporting Information Fig. S1C, S1D). Importantly, symmetric arginine methylation was not altered significantly (Fig. 1C; Supporting Information Fig. S1C).

As the next step, we assessed the expression profile of PRMT family members. Gene expression data obtained from RNA-seq in undifferentiated ESCs revealed the high level expression of PRMT1 in undifferentiated cells, suggesting its dominant role in ESCs arginine methylation (Fig. 1D). Reverse transcriptase (RT)-qPCR validation confirmed that PRMT1 is highly expressed in ESCs and its expression remained constant during neural differentiation showing a slight increase upon RA treatment (Fig. 1E). Other type I PRMTs, responsible for aDMA were less abundant in ESCs, but PRMT2, PRMT6, and PRMT8 showed significantly increased gene expression in differentiated neurons. In line with the unaltered sDMA level, expression of type II PRMT5 was not changed (Fig. 1E).

Importantly, we found that asymmetric arginine dimethylation of Histone 4 arginine 3 (H4R3me2a) also indicated increased asymmetric arginine methylation upon differentiation (Fig. 1F). H4R3me2a mark and the identified Sam68 methylation are deposited by PRMT1 and its closest paralog PRMT8 [25, 34], however, their functional redundancy is not understood yet. These results drew our attention to the importance of PRMT1 and PRMT8 in neurogenesis. PRMT1 maintained a more or less even protein level during the

Figure 1. Asymmetric arginine methylation is changing in distinct stages of RA-induced neural differentiation. **(A):** Flow diagram of the multistage differentiation procedure that involves: (I) undifferentiated stem cell culture, (II) embryoid body formation, (III) all-trans RA treatment, and (IV) neuronal culture on poly-L-ornithin/laminin-coated plates. Indicated stages are shown with bright field microscopy. Scale bar = 40 μm. **(B):** Typical single-cell voltage clamp and current clamp measurements of terminally differentiated (day 16) neurons. Upper panel: Voltage-gated inactivating and noninactivating inward currents (from −30 mV) are marked on the figure. Lower panel: Embryonic stem cell (ESC)-derived neurons were used in depolarizing current injection steps. Alkaline phosphatase trains with overshoot are shown. **(C):** Immunoblot analysis of different stages of neural differentiation. Samples were collected at day 0, 4, 8, 12, and 16 of neural differentiation. Anti-ASYM24 antibody recognizes proteins that contain arginines that are asymmetrically dimethylated. Anti-SYM11 antibody recognizes proteins that contain arginines that are symmetrically dimethylated. GAPDH serves as a loading control. **(D):** Genome browser view of the merge of mouse ESC RNA-seq, and RNA Pol and H3K27ac ChIP-seq activity on the indicated loci. **(E):** Expression profile of PRMTs as detected by reverse transcriptase quantitative polymerase chain reaction. RNA samples were collected at day 0 (I), day 4 (II), day 8 (III), and day 12 (IV). Gene expression data are expressed as a ratio of the indicated genes' transcript relative to Gapdh. **(F):** Total intranuclear levels of histone 4 arginine 3 asymmetric dimethylation as compared by indirect immunofluorescence, on a cell-by-cell basis, by laser scanning cytometry. The columns show the means of the fluorescence intensity distribution histograms obtained for G1 cells in four independent experiments ($p \leq .001$). The bars on the columns are SDs. **(G):** Immunoblot analysis of different stages of neural differentiation. Samples were collected at day 0, day 4, day 8 (± RA treatment), and day 12 (± RA treatment). GAPDH serves as a loading control. **(H):** Localization of H4R3me2a, PRMT1, and PRMT8 (each in red) in stem cell derived neuronal cells as detected by immunocytochemistry. Neurons were costained by anti-TUJ1 antibody (green). Arrows indicate the cytoplasmic localization of PRMT1. Scale bar = 5 μm. ns, non significant; *, $p \leq .05$; **, $p \leq .01$; ***, $p \leq 0.001$. Abbreviations: atRA, all-trans Retinoic Acid; aDMA, asymmetric dimethylarginine; FBS, fetal bovine serum; LIF, leukemia inhibitory factor; MMA, monomethylarginine; PRMT, protein arginine methyl transferase; βME, beta-mercaptoethanol; RA, retinoic acid; sDMA, symmetric dimethylarginine.

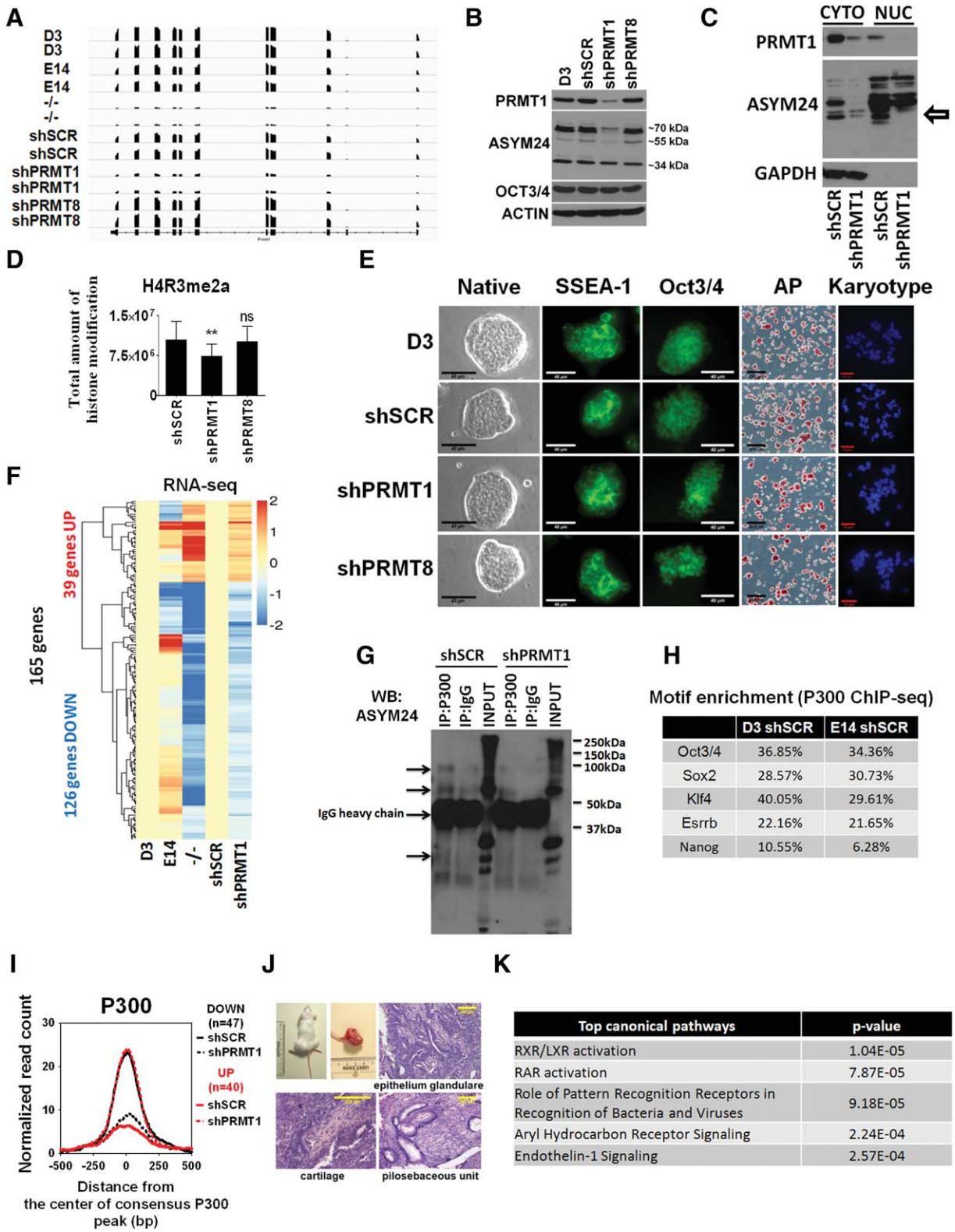

	D3 shSCR	E14 shSCR
Oct3/4	36.85%	34.36%
Sox2	28.57%	30.73%
Klf4	40.05%	29.61%
Esrrb	22.16%	21.65%
Nanog	10.55%	6.28%

Top canonical pathways	p-value
RXR/LXR activation	1.04E-05
RAR activation	7.87E-05
Role of Pattern Recognition Receptors in Recognition of Bacteria and Viruses	9.18E-05
Aryl Hydrocarbon Receptor Signaling	2.24E-04
Endothelin-1 Signaling	2.57E-04

Figure 2.

course of RA-dependent neural differentiation, while PRMT8 was induced upon RA treatment and was present only in differentiated neurons (Fig. 1G). H4R3me2a and PRMT8 showed nuclear localization, while PRMT1 could also be detected in the cytoplasm of differentiated neurons (Fig. 1H).

PRMT1 Is Responsible for Arginine Methylation in ESCs and Affects Transcription

As a next step we established PRMT1 and PRMT8 knockdown ESCs to get functional insights into the role of these two proteins in neurogenesis. Although PRMT1 knockout ESCs were established previously [17], a proper genetic control was not available for comperative studies. Thus, we established PRMT1 and PRMT8 knockdown ESCs using shRNA-based gene silencing (Fig. 2A, 2B; Supporting Information Fig. S2A–S2F) in addition to PRMT1 knockout cells (Supporting Information Fig. S2G). Analysis of asymmetrically arginine dimethylated proteins using anti-ASYM24 antibody revealed hypomethylation of certain cellular proteins in PRMT1-depleted ESCs (Fig. 2B; Supporting Information Fig. S2G). PRMT1 was mainly localized in the cytoplasmic fraction, however asymmetric arginine methylation was more abundant in the nucleus (Fig. 2C; Supporting Information Fig. S1C). ASYM24 decorated signal intensity decreased in both fractions as the result of PRMT1 silencing. The total amount of PRMT1 mediated H4R3me2a histone modification was also decreased (Fig. 2D), further demonstrating the functional consequences of the loss of PRMT1 activity and indicating the role of PRMT1 in the regulation of chromatin. PRMT1-depleted or knockout cells showed typical ESC morphology and positive staining for well-established markers of pluripotency (Fig. 2E; Supporting Information Fig. S2H).

To clarify the transcriptional consequences of the reduced level of PRMT1 in ESCs, we carried out global transcriptional analyses using RNA-seq. Pathway analysis clarified that the 165 differentially expressed genes are mainly related to cellular movement (Hspb1, Fgfbp1, Ctgf, Cyr61), proliferation and p53-signaling (Camk2n1, Igfbp3, Smad7, Tpm1), tight junction, and cytoskeletal elements (Myl9, Thbs1, Sepp1) (Fig. 2F; Supporting Information Table 1). A role for PRMT1 in many of these cellular function has been previously suggested in other cellular model systems [35, 36]. Importantly, typical pluripotency markers were not affected by the loss of PRMT1, suggesting that PRMT1 in contrast to CARM1, is not required for the maintenance of pluripotency [14]. Importantly, 39 out of 165 significantly regulated genes showed upregulation in PRMT1 depleted ESCs versus control cells, suggesting the loss of repression on these genes in hypomethylated cells (Fig. 2F). Taken together, data obtained from gene-expression analysis indicate that PRMT1, beside its known transcriptional coactivator function, has a repressive feature on a set of genes, which might be relevant in various cellular functions.

Importance of arginine methylation of coregulators was demonstrated by others [37, 38]. It has been also shown that methylation of Arg3 on H4 tail peptides facilitates P300-mediated histone acetylation in vitro [21–23]. In order to see whether P300 and PRMT1 are present in one complex in ESCs we carried out coimmunprecipitation experiments. Several asymmetrically arginine methylated proteins were coimmunprecipitated along with P300 but not with the isotope control (Fig. 2G). Moreover, the asymmetric arginine methylation of these proteins were PRMT1-dependent.

To understand the contribution of PRMT1-mediated arginine methylation in P300-mediated transcriptional and epigenetic program of ESCs we determined the P300 cistrome in the presence and absence of PRMT1. We could identify 3,420 consensus P300 binding sites present in both D3 and E14 control ESCs (Supporting Information). Motif analysis revealed that P300 is mainly recruited to the stem cell specific transcription factor Oct3/4, Sox2, Klf4, Esrrb, and Nanog (Fig. 2H). Considering only those P300 bindings that were detectable and significant in both D3 and E14 cells between control and PRMT1-depleted cells we could identify only approximately 90 genomic regions. Half of these regions showed increased

Figure 2. PRMT1 is responsible for arginine methylation in embryonic stem cells (ESCs) and affects transcription. **(A):** Genome browser view of RNA-seq data comparing the PRMT1 coding locus in the indicated ESCs. Biological duplicates are shown. **(B):** Immunoblots of protein samples from the indicated D3 ESCs lines probed for expression of PRMT1, ASYM24, and OCT3/4. ACTIN was used as a loading control. **(C):** WB analysis of subcellular fractionations. Cytoplasmic (CYTO) and nuclear fractions (NUC) of undifferentiated shSCR and shPRMT1 ESCs were isolated and probed for PRMT1 and ASYM24. GAPDH is a loading control for cytoplasm. **(D):** Total intranuclear levels of H4R3 asymmetric dimethylation as compared by indirect immunofluorescence between undifferentiated shSCR and shPRMT1 ESCs. **(E):** Characterization of unmodified D3, shSCR, shPRMT1, and shPRMT8 ESCs. Expression of ESC marker SSEA-1 and OCT3/4 were determined by immunocytochemistry. AP staining show undifferentiated colonies. Chromosome counting was performed as described in the Supporting Information. Scale bar = 40 μm for Native, SSEA-1, and Oct3/4; 200 μm for AP, and 10 μm for karyotype. **(F):** Heatmap display of gene expression data of D3, E14, and PRMT1−/− ESCs, normalized to D3 and shSCR vs. shPRMT1 ESCs, normalized to shSCR. Total RNA was isolated from undifferentiated ESCs and RNA-seq experiment was carried out to determine those genes that were significantly (FDR $\leq$ 0.1 and Log2FC $\geq$1.2) upregulated ($n = 39$, red) or downregulated ($n = 126$, blue) in both PRMT1−/− and shPRMT1 ESCs vs. their control. See also Supporting Table 1. **(G):** Asym24 immunoblot of P300 interacting complex. Nuclear extract of control and PRMT1-depleted cells were used to coimmunprecipitate proteins with anti-P300 or IgG isotype control. **(H):** De novo identification of motifs under peaks from P300 ChIP-seq data using Homer. Top 1,000 binding sites in each samples and the matrix files of the best motifs (highest score) were used for forced motif search in D3 shSCR and E14 shSCR P300 ChIP-seq samples. % refers to the ratio of peaks having the given motif. **(I):** Histogram of PRMT1-dependent P300-binding. P300 ChIP-seq was carried out in shSCR and shPRMT1 D3 and E14 ESCs. Regions showing significantly different ($p < .05$) P300 occupany between shSCR and shPRMT1 in both D3 and E14 were identified by differential binding analysis, resulting 40 upregulated (red) and 47 downregulated (black) P300 occupied genomic regions in shPRMT1 (dashed line) vs. shSCR (continual line). **(J):** Hematoxylin and eosin staining of teratoma derived from PRMT1−/− ESCs. Cells were injected into lower leg of SCID mice at a concentration of 5×10^6 cells per ml. After 4–6 weeks the teratoma were surgically dissected, fixed, embedded in paraffin, and sectioned. Scale bar = 200 μm. **(K):** Ingenuity pathway analysis of genes differentially expressed at day 4. Microarray experiment was carried out using RNA samples obtained from shSCR and shPRMT1 ESCs differentiated for 4 days. Top biological functions predicted by the software and p values are shown. ns, non significant; **, $p \leq .01$. Abbreviations: AP, alkaline phosphatase; PRMT, protein arginine methyl transferase; CYTO, cytoplasmic; NUC, nuclear; RAR, Retinoic Acid Receptor; RXR, Retinoid X Receptor; WB, Western blot.

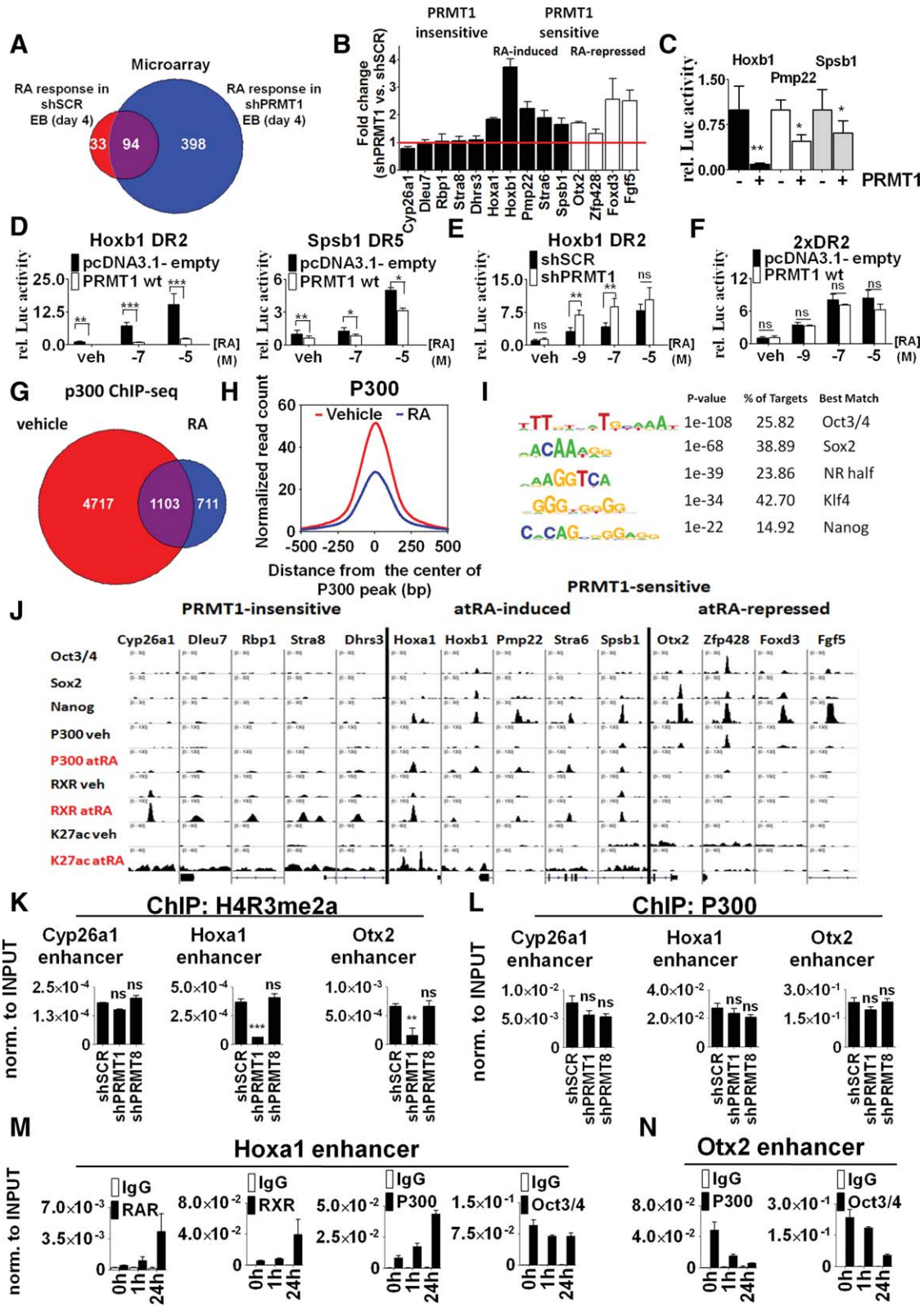
A
Microarray
RA response in shSCR EB (day 4)
RA response in shPRMT1 EB (day 4)
33
94
398
B
PRMT1 insensitive
PRMT1 sensitive
RA-induced
RA-repressed
Fold change (shPRMT1 vs. shSCR)
Cyp26a1
Dleu7
Rbp1
Stra8
Dhrs3
Hoxa1
Hoxb1
Pmp22
Stra6
Spsb1
Otx2
Zfp428
Foxd3
Fgf5
C
Hoxb1
Spsb1
Pmp22
rel. Luc activity
PRMT1
D
Hoxb1 DR2
pcDNA3.1- empty
PRMT1 wt
Spsb1 DR5
E
Hoxb1 DR2
shSCR
shPRMT1
F
2xDR2
pcDNA3.1- empty
PRMT1 wt
veh
[RA] (M)
G
p300 ChIP-seq
vehicle
RA
4717
1103
711
H
P300
Vehicle
RA
Normalized read count
Distance from the center of P300 peak (bp)
I
P-value
% of Targets
Best Match
1e-108 25.82 Oct3/4
1e-68 38.89 Sox2
1e-39 23.86 NR half
1e-34 42.70 Klf4
1e-22 14.92 Nanog
J
PRMT1-insensitive
atRA-induced
PRMT1-sensitive
atRA-repressed
Oct3/4
Sox2
Nanog
P300 veh
P300 atRA
RXR veh
RXR atRA
K27ac veh
K27ac atRA
K
ChIP: H4R3me2a
L
ChIP: P300
Cyp26a1 enhancer
Hoxa1 enhancer
Otx2 enhancer
norm. to INPUT
shSCR
shPRMT1
shPRMT8
M
Hoxa1 enhancer
IgG
RAR
RXR
P300
Oct3/4
0h
1h
24h
N
Otx2 enhancer

Figure 3.

P300 occupancy in PRMT1 knockdowns (Fig. 2I). We could identify only few examples where PRMT1-dependent P300 recruitment were coupled to differential gene expression (e.g., Igsf21, Ankrd35, Sema3e, Colec12). These results suggest that, at least in undifferentiated ESCs, P300 occupancy is dominantly PRMT1-independent.

We next evaluated the differentiation potential of the PRMT1-depleted cells. Genome-wide comparison and RT-qPCR validation of spontaneously differentiated control and hypomethylated cells showed that classical lineage markers of endoderm, mesoderm, and ectoderm were similarly induced upon spontaneous differentiation (Supporting Information Fig. S3A–S3C). Injection of PRMT1−/− ESCs into immunodeficient mice resulted in teratoma formation with obvious differentiated structures from all three germinal layers, excluding the possibility that residual PRMT1, present in knockdown cells, is sufficient for differentiation (Fig. 2J). PRMT1−/− cells were also able to differentiate to Vimentin+ mesenchymal cells and TroponinC+ cardiomyocytes (Supporting Information Fig. S3D), suggesting that cells can undergo differentiation to various cell types in the absence of PRMT1.

To identify differentiation-related signaling pathways that were affected in hypomethylated cells, we compared the gene expression profile at day 4 of differentiation. Pathway analysis based on altered expression of Dusp1, Fos, Smad3, and Tgfb3 predicted RXR:LXR and RXR:RAR activation as one of the top canonical pathways being reactivated in the absence of PRMT1 (Fig. 2K).

PRMT1 Selectively Modulates the Regulation Retinoid Target Genes

RA, acting through the activation of RXR:RAR, is a general inducer of ESCs differentiation [39]. In order to characterize the early response of RA in PRMT1-depleted cells, we performed genome-wide comparison of gene expression in RA-treated EBs (day 4). 12 hours of RA treatment changed the expression of 127 genes in control cells and 492 genes in hypomethylated cells (Fig. 3A). While most of the known retinoid targets, such as Cyp26a1, Dhrs3, Dleu7, Rbp1, Stra8 were induced to the same degree in PRMT1-depleted and control cells; Hoxa1, Hoxb1, Stra6, Pmp22, and Spsb1 also under RA control [40, 41], showed higher induction in hypomethylated cells (Fig. 3B; Supporting Information Figs. S4, S5A, S5B). Importantly, many genes (e.g., Foxd3, Otx2) showed more pronounced RA-induced repression in PRMT1 knockdown cells, while Zfp428 and Fgf5 were only repressed in PRMT1-depleted cells (Fig. 3B; Supporting Information Fig. S4). These results suggest a gene-selective regulatory effect of PRMT1 in the RA response of ESCs.

To further investigate the selectivity at the promoter level, we transfected ESCs with the Hoxb1 promoter, containing the DR2 RA-response element, linked to a luciferase reporter gene [41] (Supporting Information Fig. S5C). Transient overexpression of PRMT1 resulted in a decrease in basal transcription level of Hoxb1 (Fig. 3C). To a lesser extent Pmp22 and Spsb1 enhancers were also suppressed in the presence of PRMT1. The ligand induced retinoid response of Hoxb1 and Spsb1 were also decreased (Fig. 3D). Accordingly, in the absence of PRMT1, RA-dependent transcriptional activity was markedly increased (Fig. 3E). Importantly, PRMT1 had no effect in case of a synthetic canonical DR2 response element (Fig. 3F), suggesting a context-dependent and promoter-selective effect of PRMT1 in the regulation of retinoid response.

P300 has been implicated as a regulator of retinoid response in F9 cells [42, 43]. In order to see, whether PRMT1-modulated, RA-induced gene expression correlates with P300 binding, we first determined the RA-dependent P300 cistrome in ESCs. Upon RA treatment there was a threefold reduction in the number of P300 binding sites in control cells (Fig. 3G) and also the occupancy was substantially decreased (Fig. 3H). We could observe similar P300 redistribution in the PRMT1 knockdown cells (Supporting Information Fig. S6A).

Figure 3. PRMT1 acts as selective regulator of retinoid regulated genes. **(A):** Proportional Venn-diagram that represents the overlap between gene expression changes in retinoid induced differentiation of control (shSCR) and PRMT1-depleted cells as determined by microarray. EBs at day 4 were treated with DMSO or 5 μM RA for 12 hours. **(B):** Gene expression changes from control and PRMT1-depleted cells upon RA treatment. Cells were spontaneously differentiated for 4 days and then treated with RA or vehicle for 12 hours. Fold inductions were calculated from per chip normalized microarray data (vehicle vs. RA treated, $n = 3$ per condition) for each gene. Calculated values of PRMT-depleted cells then were normalized by values of the control. Red line shows when the induction is equal in both cell types (e.g., Cyp26a1, Dhrs3). **(C):** PRMT1-dependent repression of RA-induced enhancers. pcDNA.3.1-PRMT1 (PRMT1) or empty pcDNA3.1 (empty) plasmids were cotransfected with NHf290-Hoxb1-Luciferase plasmid [41] or Pmp22 and Spsb1 enhancers cloned into Luciferase encoding vector (Supporting Information Fig. S5C). Luciferase signal intensity was determined and normalized to βgal signal. **(D):** RA-dependent activation of Hoxb1 promoter and Spsb1 enhancer. Indicated plasmids were cotransfected with NHf290-Hoxb1-Luciferase or Spsb1-Luciferase plasmid and cells were treated with RA. **(E):** NHf-Hoxb1-Luciferase plasmid was transfected into shSCR or shPRMT1 cells. Cells were treated with RA for 24 hours using the indicated ligand concentration and normalized luciferase values determined. **(F):** DR2 RA response element containing luciferase plasmid was cotransfected with pcDNA3.1-empty or pcDNA3.1-PRMT1 expression vector. Cells were treated with RA for 24 hours using the indicated concentrations. Normalized luciferase activity was determined and the mean of triplicate determinations ± SD is shown. **(G):** Area-proportional Venn-diagram of RA induced P300 redistribution. Cistromes of P300 were determined in control (vehicle) and RA-treated (1 μM, 24 hours) D3 shSCR ESCs by ChIP-seq. **(H):** Histogram of the genome-wide occupancy of common P300 peaks ($n = 1{,}103$) in vehicle and RA-treated (1 μM, 24 hours) cells, centralized to common P300 occupied regions. **(I):** De novo identification of motifs under P300 peaks from ChIP-seq data using Homer. P300 occupied genomic regions were identified in promoter regions of the 398 PRMT1-sensitive RA-regulated genes (A). % of targets refers to the ratio of peaks having the given motif. **(J):** Genome browser view of the indicated ChIP-seq data on PRMT1-sensitive and PRMT1-insensitive loci. H3K27ac, RXR, and P300 ChIP-seq data were obtained from untreated ESCs and cells treated with 1 μM RA for 24 hours. **(K):** H4R3me2a ChIP-qPCR signals on the indicated individual enhancers (J) as detected in untreated shSCR, shPRMT1, and shPRMT8 ESCs. **(L):** P300 ChIP-qPCR signals on the indicated individual enhancers as detected in untreated shSCR, shPRMT1, and shPRMT8 ESCs. **(M):** RAR, RXR, P300, and Oct3/4 ChIP-qPCR signals on the Hoxa1 enhancer (Fig. 3J) in undifferentiated and RA-treated ESCs. **(N):** P300 and Oct3/4 ChIP-qPCR signals on the Otx2 enhancer (J) in undifferentiated and RA-treated ESCs. ns, non significant; *, $p \leq .05$; **, $p \leq .01$; ***, $p \leq .001$. Abbreviations: atRA, all-trans Retinoic Acid; ChIP, chromatin immunoprecipitation; DR, direct repeat; EB, embryoid body; Luc, luciferase; PRMT, protein arginine methyl transferase; RA, retinoic acid; RAR, Retinoic Acid Receptor; RXR, Retinoid X Receptor; wt, wild-type; veh, vehicle.

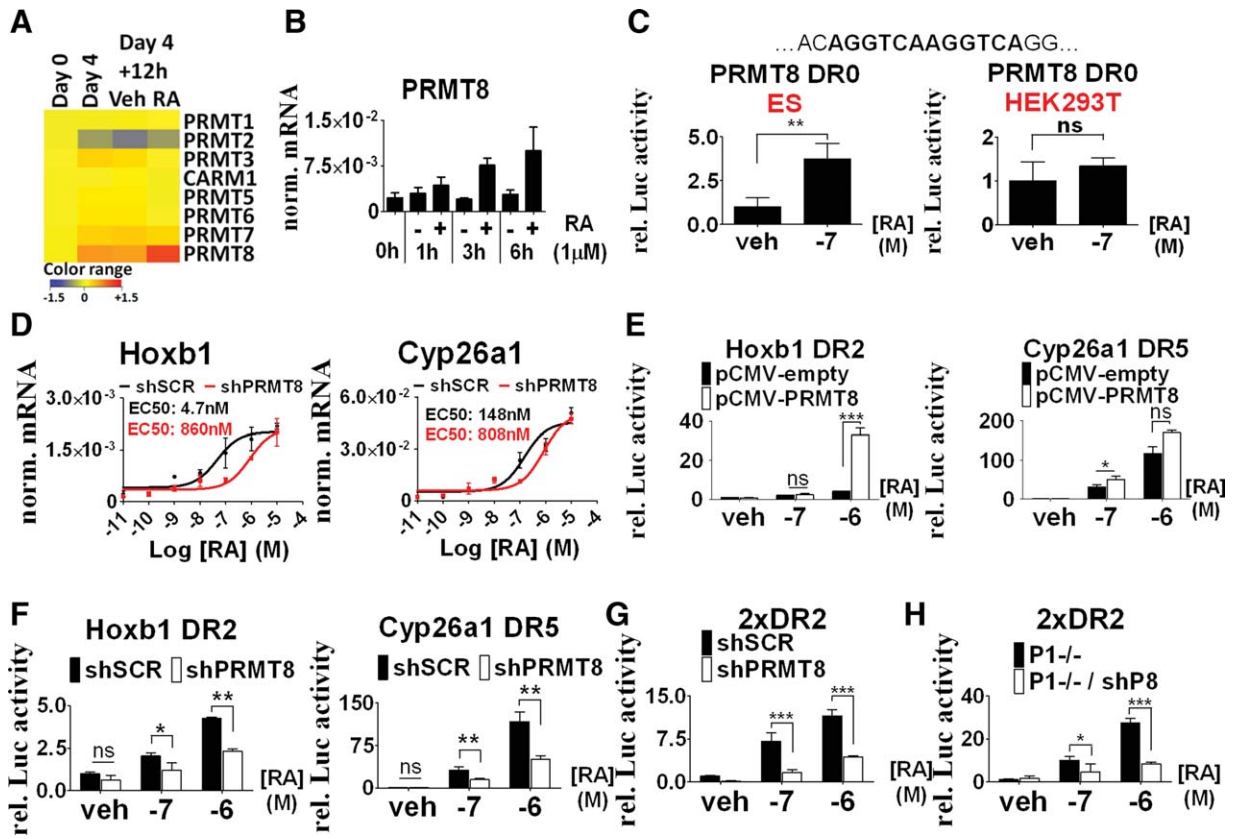

Figure 4. PRMT8 is a retinoic acid receptor regulated gene and acts as a coactivator of retinoid signaling. **(A):** Heatmap analysis of gene expression microarray data of PRMT family members. Values are normalized to undifferentiated ESCs (day 0). **(B):** Ligand response of PRMT8 upon RA treatment at various time points. Undifferentiated ESCs were treated for the indicated times with 1 μM RA.Values are expressed as mean of technical triplicates ± SD of the mean. **(C):** TK-Luc-PRMT8 was constructed by cloning 300 bp promoter region of PRMT8, containing the DR0 element, into a TK-Luc-empty plasmid. ESCs or HEK293T cells were transiently transfected and treated with 0.1 μM RA for 24 hours. Above the identified DR0 element and surrounding sequence is shown. **(D):** Dose response curves of Hoxb1 and Cyp26a1 as measured by reverse transcriptase quantitative polymerase chian reaction. shSCR and shPRMT8 ESCs were treated with the indicated concentrations of RA for 24 hours. EC50 values are shown. **(E):** TK-Luc Hoxb1 or TK-Luc Cyp26a1 enhancer traps were constructed by cloning 300 bp regions of Hoxb1 and Cyp26a1, respectively (Supporting Information Fig. S5D). ESCs were transfected along with pCMV-Tag2-empty or pCMV-Tag2-PRMT8 expression plasmid. Cells were treated with RA for 24 hours using the indicated ligand concentrations. **(F):** Hoxb1 (DR2) or Cyp26a1 (DR5) enhancer trap was transfected into shSCR or shPRMT8 ESCs. Cells were treated with RA for 24 hours using the indicated ligand concentrations. **(G):** 2x DR2 retinoic acid response element containing luciferase plasmid was transfected into shSCR or shPRMT8 ESCs. Cells were treated with RA for 24 hours using the indicated ligand concentrations. **(H):** 2x DR2 retinoic acid response element containing luciferase plasmid was transfected into PRMT1 knockout (P1−/−) or shPRMT8 PRMT1 double "knockout" (P1−/− shP8) ESCs. Cells were treated with RA for 24 hours using the indicated ligand concentrations. Normalized luciferase values were determined, and the mean of three determinations ± SD are shown. ns, non significant; *, $p \leq .05$; **, $p \leq .01$; ***, $p \leq .001$. Abbreviations: ESC, embryonic stem cell; EC50, half maximal effective concentration; DR, direct repeat; P1−/− /shP8, PRMT, protein arginine methyl transferase; PRMT1 knockout/shPRMT8; RA, retinoic acid.

P300 occupancy highly correlates with active enhancers [44]. As a next step, we identified the P300 occupied genomic regions in the close proximity of the 398 PRMT1-sensitive RA regulated genes (Fig. 3A) to identify putative common master regulators of these genes. The motif analysis of these genomic regions revealed binding site enrichment of Oct3/4, Sox2, and Nanog beside the RAR:RXR bound NR half site (Fig. 3I). Interestingly, comparison of promoter regions of PRMT1-insensitive (e.g., Cyp26a1, Dleu7, Rbp1, Stra8, Dhrs3) and PRMT1-sensitive (e.g., Hoxa1, Hoxb1, Spsb1, Pmp22, Stra6 and Foxd3, Otx2, Zfp428, Fgf5) genes showed remarkable differenes in the overall binding site enrichment for Oct3/4, Sox2, and Nanog (Fig. 3J). Moreover, P300 redistribution could also only be detected on promoter region of PRMT1-sensitive genes (Fig. 3J; Supporting Information Fig. S6B, S6C), suggesting that P300 and PRMT1 are likely to coregulate such transcriptional "hotspots."

To get further mechanistic evidence that these regions are targeted by PRMT1, we determined the H4R3me2a signal in the proximity of PRMT1-sensitive and insensitive genes. As shown in Figure 3K and Supporting Information Figure S6D, Hoxa1, Spsb1, Otx2, and Zfp428 enhancers showed clear PRMT1-dependent enrichment of H4R3me2a at these regions, while P300 recruitment was not altered (Fig. 3L; Supporting Information Fig. S6E). RA-dependent changes showed no clear tendency between the compared regions (Supporting Information Fig. S6F, S6G). In accordance with the P300 ChIP-seq data ChIP-qPCR validation confirmed that RA treatment selectively increased the recruitment of P300 to the promoter of Hoxa1 but not to Cyp26a1 or Dhrs3 (Fig. 3M; Supporting Information

Fig. S6H, S6I). Spsb1 already showed increased P300 binding which was not further enhanced (Fig. 3J) As expected, Otx2 and Zfp428 showed decreased P300 binding upon RA treatment (Supporting Information Fig. S6H, S6I). Interestingly, we detected a constant Oct3/4 binding on the Hoxa1 enhancer even after 24 hours of RA treatment (Fig. 3M), while Oct3/4 occupancy has significantly decreased on the enhancer of repressed Otx2 (Fig. 3N). These data collectively suggest that RA regulated enhancers can be grouped into two categories, PRMT1 sensitive and insensitive ones with distinct

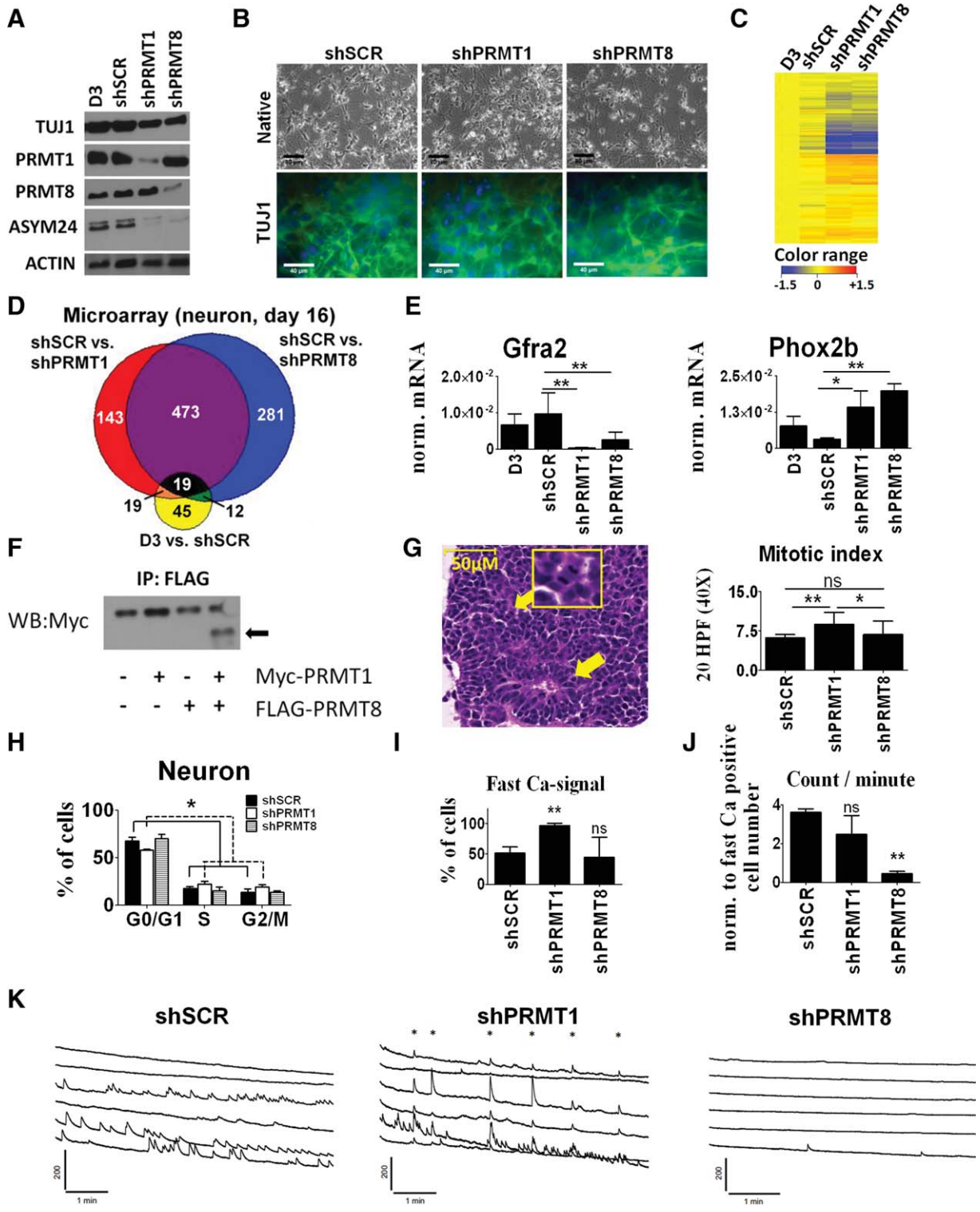

Figure 5.

transcription factor complexes. The PRMT1 sensitive ones are characterized by PRMT1-dependent H4R3me2a, Oct3/4, Sox2, Klf4, or Nanog (OSKN), and P300 binding.

PRMT8 Is a RA Inducible Coactivator of Retinoid Signaling

As it was shown in Figure 1C, RA treatment resulted in changes in asymmetric arginine methylation. Comparison of the expressional profile of PRMTs upon short-term RA-induction of day 4 EBs revealed the early upregulation of PRMT8 (Fig. 4A, 4B). To prove that PRMT8 is regulated in a RA-dependent manner, ESCs were treated with RAR and RXR specific ligands. PRMT8 expression could be induced by RAR-specific ligand AM580, but the RXR-specific LG268 had no effect (Supporting Information Fig. S7A). Moreover, RA-dependent induction of PRMT8 showed a similar time- and dose dependence as Hoxb1 and Cyp26a1, well established direct targets of the retinoid signaling pathway (Fig. 4B; Supporting Information Fig. S7B, S7C) [45]. A recently published RAR ChIP-seq in F9 cells [46] allowed us to identify a putative enhancer in the promoter region of PRMT8. This region (−1,400 to −1,450 relative to transcription start site) contains a direct repeat with no spacer (AGGTCAAGGTCA, DR0) that can bind RAR:RXR (Supporting Information Fig. S7D). Transfecting an enhancer trap vector that contains this 300-bp genomic region of the PRMT8 promoter, we could validate functionally the element in response to RA treatment in ESCs (Fig. 4C). These results confirm PRMT8 as a direct RA-regulated gene. Importantly, using the same construct, we could not detect RA-dependent induction of PRMT8 in HEK293T cells (Fig. 4C). This suggests a more complex scenario, where the presence of additional cell-type specific factors are required for proper enhancer activity.

PRMT1 and PRMT8 exhibit high sequence similarities [25], thus we were interested whether loss of PRMT8 may also affect retinoid response. Unexpectedly, loss of PRMT8 had an inhibitory effect on the retinoid response. In a dose-curve comparison of Hoxb1 and Cyp26a1, induction loss of PRMT8 resulted in a significant increase in the half maximal effective concentration (EC50) value of RA (Hoxb1: 4.8 to 860 nM, Cyp26a1: 148 to 808 nM) (Fig. 4D). To validate the coregulatory function of PRMT8 in RAR:RXR signaling, enhancer trap vectors of Hoxb1 or Cyp26a1 RARE were used in a luciferase reporter assay (Supporting Information Fig. S5D). As shown in Figure 4E, ESCs transfected with the reporter alone showed RA-dependent induction, which was further stimulated by cotransfection of PRMT8. In contrast, loss of PRMT8 resulted in a decreased signal intensity (Fig. 4F). Moreover, the decrease observed in PRMT8-depleted cells could be restored by the overexpression of PRMT8 (Supporting Information Fig. S7E). In contrast to PRMT1, loss of PRMT8 also resulted in a decrease in the signal when an artificial canonical DR2 containing reporter was used (Fig. 4G), suggesting that PRMT8 is a general coactivator of RA signaling. To dissect the role of PRMT1 and PRMT8, we used PRMT8-depleted cells on PRMT1−/− background (double knockdown). The inhibitory effect in the absence of PRMT8 was found to be independent of the presence of PRMT1 (Fig. 4H).

PRMT1 and PRMT8 Regulate Subtype Specification of Differentiating Neural Cells

Next, we studied if loss of either or both PRMT1 and/or PRMT8 has consequences on RA-induced neuronal differentiation and/or gene expression. The stability of the knockdowns has been confirmed in differentiated neurons (Fig. 5A; Supporting Information Fig. S8A). Importantly, loss of either PRMT1 or PRMT8 resulted in hypomethylation of neurons as detected by anti-ASYM24 antibody (Fig. 5A).

At day 12 of differentiation, the knockdown derived neural cells showed similar morphology and high expression of neural markers, such as Lhx1, Pax6, or Tuj1 to wild-type cells (Fig. 5B; Supporting Information Fig. S8B). PRMT1 knockout cells could also differentiate to TUJ1+ neurons (Supporting Information Fig. S8C), further demonstrating that PRMT1 is not an essential factor in early neural differentiation. In contrast, genome-wide analysis of day 16 samples revealed dysregulation of several genes in PRMT1- or PRMT8-depleted cells (Fig. 5C). Loss of either PRMT1 or PRMT8 resulted in mainly the downregulation of genes. Interestingly, grouping of the differentially expressed genes identified that a large fraction of the genes (473 out of

Figure 5. PRMT1 and PRMT8 affect neuronal differentiation. **(A):** Immunoblot analysis of day 16 differentiated neurons derived from the indicated cell types probed for the indicated proteins. **(B):** TUJ1-staining of day 12 neurons. DAPI costaining was used to visualize cell nuclei. Scale bar, black = 80 μm, white = 40 μm. **(C):** Heatmap display of microarray gene expression data obtained from D3, shSCR, shPRMT1, and shPRMT8-derived neurons at day 16, normalized to D3 neurons. Hierarchical cluster analysis is shown. Blue color indicates downregulated, red shows upregulated genes compared to D3-derived neurons. **(D):** Area-proportional Venn-diagram compares PRMT1-dependent and PRMT8-dependent gene expression changes in differentiated neurons. Cells differentiated for 16 days were used for microarray experiments. Significantly changing genes (FC ≥ 1.5, $p < .05$) were determined by comparing shSCR vs. shPRMT1 or shSCR vs. shPRMT8-derived neurons. **(E):** Reverse transcriptase quantitative polymerase chain reaction (RT-qPCR) validation of expression level of Phox2b and Gfra2 in the indicated cells. **(F):** Coimmunoprecipitation of PRMT1 by full-length FLAG-PRMT8. HEK293T cells were transfected with the indicated constructs. Anti-MYC antibody was used for immunoblot analysis. **(G):** Mitotic index of day 8 embryoid bodies were evaluated and compared by counting mitotic figures on H&E-stained slides. A representative mitotic figure and a rosettoid structure are shown. Average number of mitotic figures per 20 consecutive HPF (×40 magnification) is shown. **(H):** Cell cycle analysis of the differentiated shSCR, shPRMT1, and shPRMT8 knockdown cells. Nuclei of agarose embedded and permeabilized cells were stained with propidium iodide and measured by laser scanning cytometry. In the left panel, the bar charts show the percentage of cells in the different cell cycle phases. Error bars: SD calculated from $n \geq 3$ independent experiments. The dot plots and DNA histograms (right panel) show one representative measurement for each cell line. In the case of shSCR and shPRMT1 neurons, the difference between the ratio of nondividing and dividing cells ((G1+G0)/(S+G2+M)) was statistically significant ($p = .029$; Mann Whitney rank sum test). **(I):** Ratio of cells with recorded fast calcium signal. Recordings and analysis has been carried out in the indicated embryonic stem cell-derived neural cultures. A representative experiment is shown (>200 measured neurons/condition). **(J):** Counts of calcium signals per minute normalized to the number of cells with positive calcium signal. A representative experiment is shown (>200 measured neurons/condition). **(K):** Synchronous activity among the cells of the PRMT1 knockdown cultures. Synchronous events labelled with asterisks. Calcium imaging records of six randomly chosen ROIs (regions of interests) per condition are shown. ns, non significant; *, $p \leq .05$; **, $p \leq .01$. Abbreviations: HPF, high-power fields; IP, immunoprecipitation; PRMT, protein arginine methyl transferase; WB, Western blot.

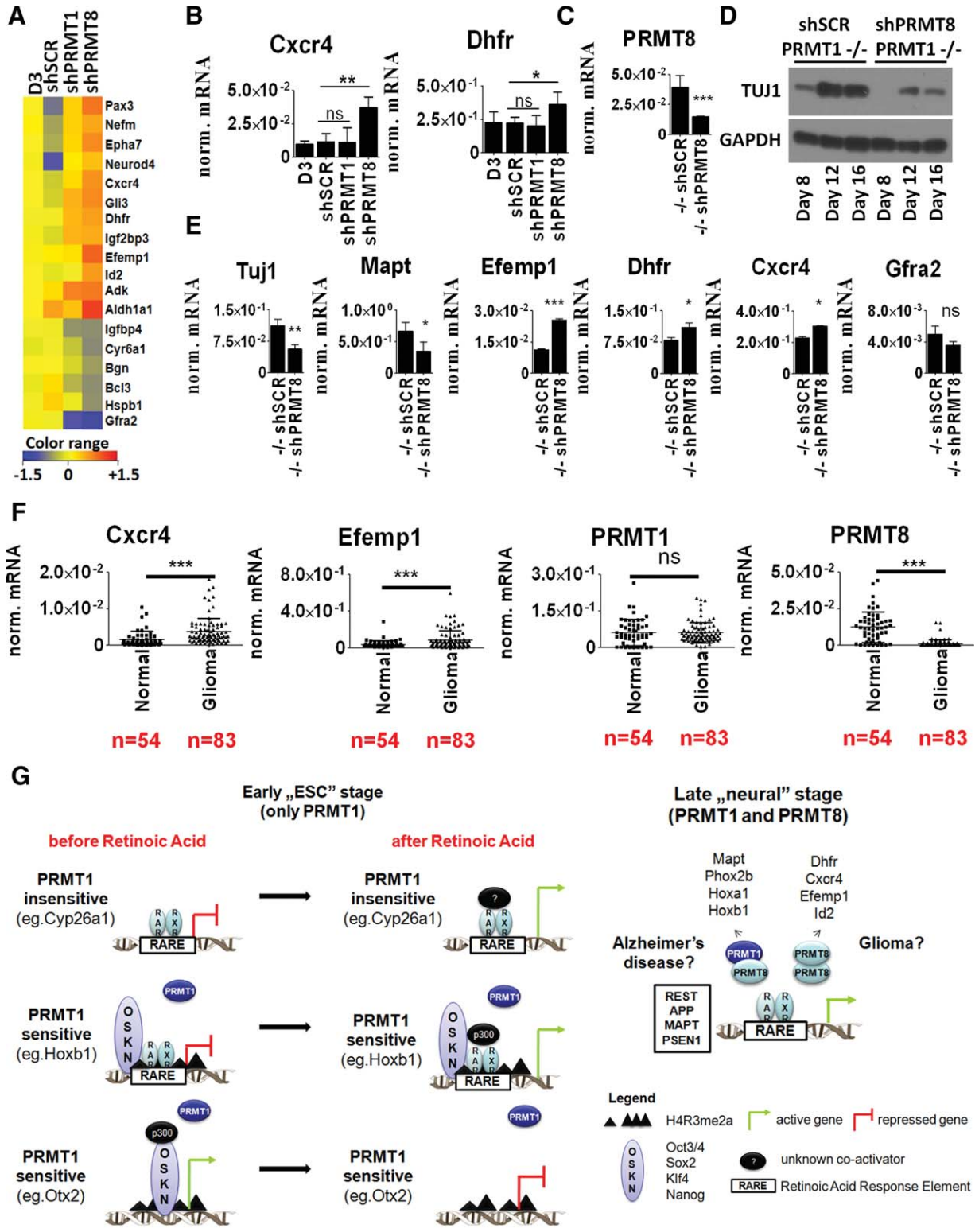

Figure 6.

947) showed similar dysregulation in both knockdown cell types (Fig. 5D). We validated Phox2b (Paired-Like Homeobox 2b), an important transcription factor of neural specification [47] and Gfra2 (GDNF Family Receptor Alpha), a regulator of neurite outgrowth [48] by RT-qPCR (Fig. 5E). Gene expression data suggested that PRMT1 and PRMT8 might act together in the regulation of these genes. Indeed, as shown in Figure 5F, coimmunoprecipitation studies confirmed that the two proteins are likely present in one complex.

To further evaluate the characteristics of early progenitors and differentiated neurons, we compared the ratio of dividing versus nondividing cells. In the progenitor phase, mitotic index of PRMT1-depleted cells were significantly higher (Fig. 5G). Cell cycle analysis of differentiated cells at day 16 also suggested that PRMT1-depleted cells show significantly higher number of nonterminally differentiated, dividing cells (Fig. 5H).

Importantly, expression level of ESC markers and mesoderm, endoderm, or early ectoderm lineage markers were similarly low in neurons differentiated from hypomethylated cells (Supporting Information Fig. S8D–S8F), further confirming that loss of PRMT1 and PRMT8 do not inhibit the neural differentiation per se. Ingenuity pathway analysis of the 473 genes (Fig. 5D) implicated PRMT1 and PRMT8 in neuronal synaptic formation, glutamate receptor signaling, and axonal guidence (Supporting Information Fig. S8G). Next, we studied functional properties of PRMT1- or 8-depleted neurons by calcium imaging. This method allowed us to compare >200 cells per condition. Importantly, the frequency of calcium peaks and the frequency of action potentials recorded in the same neuron showed a significant correlation (Supporting Information Fig. S9A), in accordance with earlier observations [28, 49, 50]. Approximetly 50% of the cells showed neural activity in the control and PRMT8 knockdown cells, while in the PRMT1-depleted cell culture the rate of active cells was almost 100% (Fig. 5I). As a remarkable difference, we found that the frequency of fast calcium signals per active cells was dramatically dropped in PRMT8-knockdowns, suggesting an important role of PRMT8 in the establishement of neuronal excitability (Fig. 5J). Another interesting observation was the frequent occurance of synchronous activity among the cells of the PRMT1 knockdown cultures (see synchronous events labeled with asterisks in Fig. 5K).

PRMT8 Regulates Distinct Set of Genes and Loss of PRMT8 Is a Marker of Glioblastoma Multiforme

The gene expressional analysis also revealed that several genes, such as Cxcr4, Dhfr, or Efemp1 previously linked to glial differentiation and gliomagenesis [51–53] were expressed differentially only in PRMT8 knockdown cells (Fig. 6A, 6B). Using PRMT1-PRMT8 double knockdown cells, we found that these genes are PRMT8-dependent (Fig. 6C–6E).

We used a large number of human primary glioma samples to confirm that PRMT8-dependent Cxcr4 and Efemp1 indeed show dysregulation in glioblastoma multiforme (GBM) (Fig. 6F). Prompted by this finding and a result of a recent study that linked Single-nucleotide polymorphism (SNP) variation in PRMT8 promoter to familial gliomagenesis [54], we also determined expression of PRMT8 in these samples. Very strikingly, PRMT8 itself showed a substantially lower expression level in GBM samples, while PRMT1 did not show a difference between the groups (Fig. 6F). These data indicate that loss of PRMT8 and genes regulated by it are putative markers in GBM and might participate in its development.

Discussion

We combined genetic approaches with genome-wide gene expression technologies to unravel the contribution of PRMT1 and PRMT8 to in vitro neuronal differentiation. We propose the following model (Fig. 6G). There are two distinct phases during the course of neural differentiation: in early stages only PRMT1 is expressed. PRMT1 acts as a selective repressor of a large set of RA-induced genes (Hoxa1, Hoxb1, Pmp22, and Spsb1). The promoter regions of these PRMT1-sensitive genes are regulatory hotspots as they are occupied by OSKN and show P300 recruitment upon RA treatment. Genes, such as Otx2 and Zfp428 that are active in ESCs and occupied by OSKN and P300 are also influenced by PRMT1. This way PRMT1 arms the cells with a negative feedback mechanism to limit RA's effect on a subset of target genes.

Subsequently, the RA signal directly induces the expression of PRMT8. In this late stage, PRMT8 collaborate with PRMT1 but PRMT8 might also exist as a homodimer [25]. PRMT8 in such complex acts as a coactivator that potentiates

Figure 6. Loss of PRMT8 results in a gene expression profile that resemble neurological disorder. **(A):** Heatmap visualization of microarray data of the indicated glioma-releated markers in ES-derived neurons. Cells differentiated for 16 days were used for microarray experiments, and data were normalized to wild type D3-derived neurons. **(B):** Gene expression level of Cxcr4 and Dhfr as measured by reverse transcriptase quantitative polymerase chain reaction (RT-qPCR) in day 16 ESC-derived neurons. **(C):** Gene expression level of PRMT8 in PRMT1−/− shSCR vs. PRMT1−/− shPRMT8 ESC-derived neurons as measured by RT-qPCR at day 12 of differentiation. **(D):** Immunoblot analysis of TUJ1 in different stages of PRMT1−/− shSCR vs. PRMT1−/− shPRMT8 neural differentiation. Samples were collected at day 8, 12, and 16. GAPDH serves as a loading control. **(E):** Gene expression level of indicated genes in PRMT1−/− shSCR vs. PRMT1−/− shPRMT8 ESC-derived neurons as measured by RT-qPCR at day 14 of differentiation. **(F):** Gene expression level of Cxcr4, Efemp1, PRMT1, and PRMT8 as measured by RT-qPCR. Human normal ($n = 54$) and glioblastoma multiforme (GBM) ($n = 83$) samples were compared. Each dot represents an individual sample. **(G):** Proposed model of PRMT1 and 8's action on early and late stage of neuronal differentiation. PRMT1 is expressed in early stage and acts as a selective repressor of retinoic acid induced gene expression. PRMT1-sensitive (e.g., Hoxb1) regions are occupied by Oct3/4, Sox2, Klf4, or Nanog, while PRMT1-insensitive sites (e.g., Cyp26a1) are not enriched for these transcription factors. P300 is also selectively recruited to the PRMT1-sensitive sites only. H4R3me2a marks can be detected in a PRMT1-dependent manner on the close proximity of all these PRMT1-sensitive enhancers. PRMT1-sensitive, retinoic acid (RA)-repressed genes (e.g., Otx2) also show P300 and OSKN occupancy in untreated ESCs. In the late stage, RA-induced PRMT8 are present in a complex with PRMT1 but PRMT8 might also exist as a homodimer [25]. PRMT8 in such complexes acts as a coactivator that potentiates retinoid response. Hox-genes, Mapt and Phox2b are regulated by both PRMT1 and PRMT8. Pathway analysis predicts REST, MAPT, APP, PSEN1 as upstream regulators responsible for dysregulated gene expression. PRMT8 has a PRMT1-independent regulatory potential as well, affecting gliomagenesis-related genes, such as Cxcr4, Dhfr, or Efemp1. ns, non significant; *, $p \leq .05$; **, $p \leq .01$; ***, $p \leq .001$. Abbreviations: ESC, embryonic stem cell; PRMT, protein arginine methyl transferase; RARE, retinoic acid response element.

retinoid response. In this way PRMT1 and its closest paralog PRMT8 integrate the morphogenic RA signal in a temporal manner acting as a rheostat. Loss of PRMT1 or PRMT8 results in mostly similar changes in neural specification, but PRMT1 and PRMT8 have independent regulatory potential as well.

PRMT1 has been previously identified as a ubiquitously expressed secondary coactivator for nuclear receptors. It has been also shown to bind the activation domain (AD2) of primary coactivators and enhance transcription [10]. In contrast to this, our results now show a repressive function of PRMT1, confirming in principle the findings of previous studies providing evidence for corepressor roles for PRMT1 in different cellular context [55, 56]. These opposing roles in gene expression regulation are not unique to PRMT1, similar phenomena have been reported in case of other coactivators as well [57].

Gene and enhancer selectivity is also a novel and striking feature of PRMT1, however the exact mechanism remains unclear. Strikingly, PRMT1-sensitive sites show characteristics of cell-type specific regulatory hotspots [58]: key transcription factors, such as Oct3/4, Sox2, Klf4, and Nanog appear to be enriched and mark these genomic regions. Importantly, the coactivator P300 is also selectively recruited to these sites upon RA treatment, providing further evidence to the existence of distinct epigenetic states between PRMT1-sensitive and -insensitive sites. We found no indication that loss of PRMT1 would affect P300 recruitment to these hotspots, but we could detect a remarkable decrease in the level of H4R3me2a mark at these sites in PRMT1-depleted cells, suggesting the presence of PRMT1 at these genomic regions. PRMT1-insensitive regions did not show PRMT1-dependent H4R3me2a enrichment, however few exceptions could be noticed (e.g., Rarβ). Due to the lack of reliable ChIP-grade anti-PRMT1 antibody, we could not get reproducible data so far which would provide direct evidence for the presence of PRMT1 at these sites though. A potential mechanism for the enhancer selective effect of PRMT1 is that P300 or a member of this protein complex is arginine methylated and this affects its coactivator function. This scenario would also explain why only P300 recruiting genomic regions are PRMT1-sensitive. Such arginine methylation-dependent regulation of CBP has been demonstrated by others [37, 38], and we also could detect the presence of arginine methylated proteins in the P300 complex. Further studies will be required to evaluate this possibility in neuronal differentiation.

The result of loss of PRMT1 function in differentiating neurons is altered gene expression. Gene expression data obtained can be used in further studies to mechanistically describe the PRMT-dependent transcriptional network in neurogenesis. Importantly, the detected gene expression differences could be linked to various functional defects. First, we found that loss of PRMT1 resulted in a delay in the cell cycle exit and elevated number of mitotically active cells. These findings are in line with a study which has identified the dominantly PRMT1-mediated H4R3me2a as a marker of postmitotic neurons [59].

A recent study identified methylation of brain sodium channel Nav1.2 in response to seizures [60]. Our preliminary comparison of electrophysiological properties of the knockdown cells led us to the conclusion that PRMT1 and PRMT8 are likely to be responsible for the proper function of ion channels. Further in vitro and animal studies will be required to identify more precisely the functional consequences of loss of these PRMTs.

Dysregulation of RA signaling has also been implicated in disease emergence and progression [61]. It is an intriguing question whether PRMT1 and PRMT8 are involved in pathological conditions of the brain as well. Our pathway analysis indicates a role of PRMT1 and PRMT8 in microtubule-associated protein tau-, amyloid beta A4 protein-, presenilin 1-, and brain-derived neurotrophic factor- related pathways. Moreover, several genes showing dysregulated expression in knockdowns have been also identified in a recent study as potential markers of human AD [62] (Supporting Information Fig. S9B, S9C). As PRMT1 or PRMT8 expression has not been investigated in such disease conditions it is still very tentative to suggest PRMT1 and PRMT8 in the progression of AD. However the observed gene expression pattern calls for further in vivo correlative as well as mechanistic studies.

A previous comparison of mammalian PRMTs revealed that PRMT1 and PRMT8 share the highest degree of identity within this enzyme family [25]. Not only the amino acid sequence of the two proteins but also the intron-exon boundaries are well conserved, suggesting that PRMT8 evolved by the duplication of PRMT1. Importantly, a recent study demonstrated that despite the similarities, PRMT1 and PRMT8 have nonredundant functions in the neural development of Zebrafish [63], suggesting that PRMT8 has acquired novel functions since its duplication. Our genome-wide screen and double knockdown experiments also provide evidence of a PRMT1-independent program of PRMT8.

Dysregulation of RA signaling has been also implicated in progression of different subtypes of cancers [64]. In a recent study, upregulation of PRMT1 has been reported in glioma tissues and glioma cell lines [65]. In order to revisit this issue we used a large patient cohort and found that the RNA levels of PRMT8 are almost completely downregulated in glioma tissues. A trivial explanation may be that PRMT8, a highly specific neural marker, is not expressed in astrocyte-derived tumors [66]. Alternatively, loss of PRMT8 positively affects astrocyte differentiation, resulting in a shift in cell fate commitment. Further in vivo and in vitro studies are required to provide evidence to this. Our results show that loss of PRMT8 results in a decrease in the level of Gfra2 and increase in the level of Cxcr4, Dhfr, and Efemp1 in single and double knockdown cells as well. These are established markers of astrocyte-derived glioma [52, 67, 68]. Furthermore, a recent genome-wide linkage study of glioma families linked a PRMT8-related SNP to gliomagenesis [54]. Downstream effect of this SNP has not been linked to the expression of PRMT8 yet. Although further work is required, these results already provide strong support to the notion that PRMT8 might be a genetic risk factor in gliomagenesis and also a putative therapeutic target. Regardless of the mechanism, our results implicate PRMT8 as a biomarker of glioma tissues.

Conclusions

In summary, the results of this study suggest a novel and so far unprecedented mechanism of how two evolutionary linked proteins with similar enzymatic activity can have distinct effects on cellular differentiation through the integration of

retinoid signaling acting as parts of a rheostat. These results provide a new conceptual framework for the interpretation of retinoid signaling in neuronal differentiation and potentially in other tissues as well. These proteins, PRMT1 and PRMT8, can also be targeted pharmacologically to modulate neuronal differentiation in vitro or in vivo and might also be a relevant target in a major unresolved clinical issues such as gliomas and Alzheimer's disease.

Acknowledgement

We acknowledge Dr. Istvan Szatmari and members of the Nagy laboratory for discussions and comments on the manuscript; Ibolya Furtos, Beata Szalka, Marta Beladi, Imrene Molnar, and Zoltanne Karolyi for technical assistance; Dr. Andras Dinnyes and Julianna Kobolak (Agricultural Biotechnology Center, Godollo, Hungary) for help with ES work. L.N is supported by a grant from the Hungarian Scientific Research Fund (OTKA K100196), TÁMOP422-2012-0023 VÉD-ELEM implemented through the New Hungary Development Plan cofinanced by the European Social Fund and the European Regional Development Fund and Hungarian Brain Research Program—Grant No. KTIA-13-NAP-A-I/9. Z.S is a recipient of TÁMOP-422/B10/1-2010-0024 grant and supported by TÁMOP 4.2.4. A/2-11-1-2012-0001/A2-JÁDJ-13. B.L.B. was supported by a grant from the Hungarian Scientific Research Fund (OTKA F68254). B.L.B. is Bolyai fellow of the HAS, Szodoray fellow of the University of Debrecen Medical and Health Science Center, and recipient of the Magyary Zoltan fellowship supported by the TÁMOP 4.2.4.A/2-11-1-2012-0001 grant. I.J. was supported by a grant from TÁMOP-4.2.2.A-11/1KONV-2012-0023. A.K. was supported by the János Bolyai stipendium and the Hungarian Brain Research Program—Grant No. KTIA_13_NAP-A-V/3. Library preparation and bioinformatic analysis was performed at the Center of Clinical Genomics and Personalized Medicine of the University of Debrecen. RNA-sequencing was performed at the Centre National de Genotypage (CNG) Paris, directed by Jean-Francois Deleuze and supported by the European Sequencing and Genotyping Infrastructure (funded by the European Commission, FP7/2007–2013) under grant agreement no. 26205 (ESGI), as part of the ADIPOMACS transnational access programme.

Author Contributions

Z.S.: conception and design, collection and/or assembly of data, data analysis and interpretation, and manuscript writing; E.C., A.H., B.D., E.B., and P.S.: data analysis and interpretation; A.K.: collection and/or assembly of data and data analysis and interpretation; C.B., S.P., L.I., G.S., S.S., K.K., I.K., G.H., L.B., and A.K.: collection and/or assembly of data; I.J.: provision of study material; B.L.B.: financial support, conception and design, and data analysis and interpretation; L.N.: conception and design, data analysis and interpretation, financial support, manuscript writing, and final approval of manuscript.

Disclosure of Potential Conflicts of Interest

The authors indicate no potential conflicts of interest.

References

1 Thaller C, Eichele G. Identification and spatial distribution of retinoids in the developing chick limb bud. Nature 1987;327:625–628.

2 Shimozono S, Iimura T, Kitaguchi T et al. Visualization of an endogenous retinoic acid gradient across embryonic development. Nature 2013;496:363–366.

3 Chambon P. The nuclear receptor superfamily: A personal retrospect on the first two decades. Mol Endocrinol 2005;19:1418–1428.

4 Koide T, Downes M, Chandraratna RA et al. Active repression of RAR signaling is required for head formation. Genes Dev 2001;15:2111–2121.

5 Glass CK, Rosenfeld MG. The coregulator exchange in transcriptional functions of nuclear receptors. Genes Dev 2000;14:121–141.

6 Rochette-Egly C. Dynamic combinatorial networks in nuclear receptor-mediated transcription. J Biol Chem 2005;280:32565–32568.

7 Lonard DM, O'Malley BW. Nuclear receptor coregulators: Judges, juries, and executioners of cellular regulation. Mol Cell 2007;27:691–700.

8 Xie Y, Ke S, Ouyang N et al. Epigenetic regulation of transcriptional activity of pregnane X receptor by protein arginine methyltransferase 1. J Biol Chem 2009;284:9199–9205.

9 Rizzo G, Renga B, Antonelli E et al. The methyl transferase PRMT1 functions as co-activator of farnesoid X receptor (FXR)/9-cis retinoid X receptor and regulates transcription of FXR responsive genes. Mol Pharmacol 2005;68:551–558.

10 Koh SS, Chen D, Lee YH et al. Synergistic enhancement of nuclear receptor function by p160 coactivators and two coactivators with protein methyltransferase activities. J Biol Chem 2001;276:1089–1098.

11 Balint BL, Szanto A, Madi A et al. Arginine methylation provides epigenetic transcription memory for retinoid-induced differentiation in myeloid cells. Mol Cell Biol 2005;25:5648–5663.

12 Gayatri S, Bedford MT. Readers of histone methylarginine marks. Biochim Biophys Acta 2014.

13 Lee YH, Ma H, Tan TZ et al. Protein arginine methyltransferase 6 regulates embryonic stem cell identity. Stem Cells Dev 2012;21:2613–2622.

14 Wu Q, Bruce AW, Jedrusik A et al. CARM1 is required in embryonic stem cells to maintain pluripotency and resist differentiation. Stem Cells 2009;27:2637–2645.

15 Nakajima T, Matsuoka Y, Kakimoto Y. Isolation and identification of N-G-monomethyl, N-G, N-G-dimethyl- and N-G,N' G-dimethylarginine from the hydrolysate of proteins of bovine brain. Biochim Biophys Acta 1971;230:212–222.

16 Miyata S, Mori Y, Tohyama M. PRMT1 and Btg2 regulates neurite outgrowth of Neuro2a cells. Neurosci Lett 2008;445:162–165.

17 Pawlak MR, Scherer CA, Chen J et al. Arginine *N*-methyltransferase 1 is required for early postimplantation mouse development, but cells deficient in the enzyme are viable. Mol Cell Biol 2000;20:4859–4869.

18 Cimato TR, Tang J, Xu Y et al. Nerve growth factor-mediated increases in protein methylation occur predominantly at type I arginine methylation sites and involve protein arginine methyltransferase 1. J Neurosci Res 2002;67:435–442.

19 Tsai YJ, Pan H, Hung CM et al. The predominant protein arginine methyltransferase PRMT1 is critical for zebrafish convergence and extension during gastrulation. FEBS J 2011;278:905–917.

20 Bedford MT, Clarke SG. Protein arginine methylation in mammals: Who, what, and why. Mol Cell 2009;33:1–13.

21 Wang H, Huang ZQ, Xia L et al. Methylation of histone H4 at arginine 3 facilitating transcriptional activation by nuclear hormone receptor. Science 2001;293:853–857.

22 Huang S, Litt M, Felsenfeld G. Methylation of histone H4 by arginine methyltransferase PRMT1 is essential in vivo for many subsequent histone modifications. Genes Dev 2005;19:1885–1893.

23 An W, Kim J, Roeder RG. Ordered cooperative functions of PRMT1, p300, and CARM1 in transcriptional activation by p53. Cell 2004;117:735–748.

24 Lee DY, Ianculescu I, Purcell D et al. Surface-scanning mutational analysis of protein arginine methyltransferase 1: Roles of specific amino acids in methyltransferase substrate specificity, oligomerization, and coactivator function. Mol Endocrinol 2007;21:1381–1393.

25 Lee J, Sayegh J, Daniel J et al. PRMT8, a new membrane-bound tissue-specific member of the protein arginine methyltransferase family. J Biol Chem 2005;280:32890–32896.
26 Bibel M, Richter J, Lacroix E et al. Generation of a defined and uniform population of CNS progenitors and neurons from mouse embryonic stem cells. Nat Protoc 2007;2: 1034–1043.
27 Martin B, Bernardon JM, Cavey MT et al. Selective synthetic ligands for human nuclear retinoic acid receptors. Skin Pharmacol 1992;5:57–65.
28 Koszeghy A, Vincze J, Rusznak Z et al. Activation of muscarinic receptors increases the activity of the granule neurones of the rat dorsal cochlear nucleus—A calcium imaging study. Pflugers Arch 2012;463:829–844.
29 Barish GD, Yu RT, Karunasiri MS et al. The Bcl6-SMRT/NCoR cistrome represses inflammation to attenuate atherosclerosis. Cell Metab 2012;15:554–562.
30 Barth L, Sutterlin R, Nenniger M et al. Functional differentiation of stem cell-derived neurons from different murine backgrounds. Front Cell Neurosci 2014;8:49.
31 Niwa H, Miyazaki J, Smith AG. Quantitative expression of Oct-3/4 defines differentiation, dedifferentiation or self-renewal of ES cells. Nat Genet 2000;24:372–376.
32 Diez del Corral R, Storey KG. Markers in vertebrate neurogenesis. Nat Rev Neurosci 2001;2:835–839.
33 Cote J, Boisvert FM, Boulanger MC et al. Sam68 RNA binding protein is an in vivo substrate for protein arginine *N*-methyltransferase 1. Mol Biol Cell 2003;14:274–287.
34 Sayegh J, Webb K, Cheng D et al. Regulation of protein arginine methyltransferase 8 (PRMT8) activity by its N-terminal domain. J Biol Chem 2007;282:36444–36453.
35 Boisvert FM, Dery U, Masson JY et al. Arginine methylation of MRE11 by PRMT1 is required for DNA damage checkpoint control. Genes Dev 2005;19:671–676.
36 Yu Z, Chen T, Hebert J et al. A mouse PRMT1 null allele defines an essential role for arginine methylation in genome maintenance and cell proliferation. Mol Cell Biol 2009;29:2982–2996.
37 Chevillard-Briet M, Trouche D, Vandel L. Control of CBP co-activating activity by arginine methylation. EMBO J 2002;21:5457–5466.
38 Ceschin DG, Walia M, Wenk SS et al. Methylation specifies distinct estrogen-induced binding site repertoires of CBP to chromatin. Genes Dev 2011;25:1132–1146.
39 Gudas LJ. Retinoids induce stem cell differentiation via epigenetic changes. Semin Cell Dev Biol 2013;24:701–705.
40 Dupe V, Davenne M, Brocard J et al. In vivo functional analysis of the Hoxa-1 3′ retinoic acid response element (3′RARE). Development 1997;124:399–410.
41 Ogura T, Evans RM. Evidence for two distinct retinoic acid response pathways for HOXB1 gene regulation. Proc Natl Acad Sci USA 1995;92:392–396.
42 Kawasaki H, Eckner R, Yao TP et al. Distinct roles of the co-activators p300 and CBP in retinoic-acid-induced F9-cell differentiation. Nature 1998;393:284–289.
43 Kashyap V, Gudas LJ. Epigenetic regulatory mechanisms distinguish retinoic acid-mediated transcriptional responses in stem cells and fibroblasts. J Biol Chem 2010;285: 14534–14548.
44 Visel A, Blow MJ, Li Z et al. ChIP-seq accurately predicts tissue-specific activity of enhancers. Nature 2009;457:854–858.
45 Simandi Z, Balint BL, Poliska S et al. Activation of retinoic acid receptor signaling coordinates lineage commitment of spontaneously differentiating mouse embryonic stem cells in embryoid bodies. FEBS Lett 2010;584:3123–3130.
46 Mendoza-Parra MA, Walia M, Sankar M et al. Dissecting the retinoid-induced differentiation of F9 embryonal stem cells by integrative genomics. Mol Syst Biol 2011;7:538.
47 Brunet JF, Pattyn A. Phox2 genes–From patterning to connectivity. Curr Opin Genet Dev 2002;12:435–440.
48 Yoong LF, Too HP. Glial cell line-derived neurotrophic factor and neurturin inhibit neurite outgrowth and activate RhoA through GFR alpha 2b, an alternatively spliced isoform of GFR alpha 2. J Neurosci 2007;27: 5603–5614.
49 Helmchen F, Imoto K, Sakmann B. Ca^{2+} buffering and action potential-evoked Ca^{2+} signaling in dendrites of pyramidal neurons. Biophys J 1996;70:1069–1081.
50 Stosiek C, Garaschuk O, Holthoff K et al. In vivo two-photon calcium imaging of neuronal networks. Proc Natl Acad Sci USA 2003;100:7319–7324.
51 Ehtesham M, Thompson RC. CXCR4-expressing glial precursor cells demonstrate enhanced migratory tropism for glioma. J Cancer Ther 2013;3:1086–1091.
52 Idbaih A, Carvalho Silva R, Criniere E et al. Genomic changes in progression of low-grade gliomas. J Neurooncol 2008;90: 133–140.
53 Huang J, Vogel G, Yu Z et al. Type II arginine methyltransferase PRMT5 regulates gene expression of inhibitors of differentiation/DNA binding Id2 and Id4 during glial cell differentiation. J Biol Chem 2011;286:44424–44432.
54 Liu Y, Melin BS, Rajaraman P et al. Insight in glioma susceptibility through an analysis of 6p22.3, 12p13.33-12.1, 17q22–23.2 and 18q23 SNP genotypes in familial and non-familial glioma. Hum Genet 2012; 131:1507–1517.
55 Kleinschmidt MA, Streubel G, Samans B et al. The protein arginine methyltransferases CARM1 and PRMT1 cooperate in gene regulation. Nucleic Acids Res 2008;36:3202–3213.
56 Lafleur VN, Richard S, Richard DE. Transcriptional repression of hypoxia-inducible factor-1 (HIF-1) by the protein arginine methyltransferase PRMT1. Mol Biol Cell 2014;25: 925–935.
57 Rogatsky I, Luecke HF, Leitman DC et al. Alternate surfaces of transcriptional coregulator GRIP1 function in different glucocorticoid receptor activation and repression contexts. Proc Natl Acad Sci USA 2002;99:16701–16706.
58 Siersbaek R, Nielsen R, John S et al. Extensive chromatin remodelling and establishment of transcription factor 'hotspots' during early adipogenesis. EMBO J 2011;30: 1459–1472.
59 Chittka A. Dynamic distribution of histone H4 arginine 3 methylation marks in the developing murine cortex. PLoS One 2010;5: e13807.
60 Baek JH, Rubinstein M, Scheuer T et al. Reciprocal changes in phosphorylation and methylation of mammalian brain sodium channels in response to seizures. J Biol Chem 2014;289:15363–15373.
61 Lee HP, Casadesus G, Zhu X et al. All-trans retinoic acid as a novel therapeutic strategy for Alzheimer's disease. Expert Rev Neurother 2009;9:1615–1621.
62 Miller JA, Woltjer RL, Goodenbour JM et al. Genes and pathways underlying regional and cell type changes in Alzheimer's disease. Genome Med 2013;5:48.
63 Lin YL, Tsai YJ, Liu YF et al. The critical role of protein arginine methyltransferase prmt8 in Zebrafish embryonic and neural development is non-redundant with its paralogue prmt1. PLoS One 2013;8:e55221.
64 Ali R, Campos B, Dyckhoff G et al. Quantification of retinoid concentrations in human serum and brain tumor tissues. Anal Chim Acta 2012;725:57–66.
65 Wang S, Tan X, Yang B et al. The role of protein arginine-methyltransferase 1 in gliomagenesis. BMB Rep 2012;45:470–475.
66 Kousaka A, Mori Y, Koyama Y et al. The distribution and characterization of endogenous protein arginine *N*-methyltransferase 8 in mouse CNS. Neuroscience 2009;163:1146–1157.
67 Hu B, Thirtamara-Rajamani KK, Sim H et al. Fibulin-3 is uniquely upregulated in malignant gliomas and promotes tumor cell motility and invasion. Mol Cancer Res 2009; 7:1756–1770.
68 do Carmo A, Patricio I, Cruz MT et al. CXCL12/CXCR4 promotes motility and proliferation of glioma cells. Cancer Biol Ther 2010;9:56–65.


See www.StemCells.com for supporting information available online.

